A COMPARISON OF THEORETICAL Si VIII EMISSION LINE RATIOS WITH OBSERVATIONS FROM SERTS

F. P. KEENAN[1], A. C. KATSIYANNIS[1], C. A. RAMSBOTTOM[2], K. L. BELL[2], J. W. BROSIUS[3,4], J. M. DAVILA[3] and R. J. THOMAS[3]

[1]*Department of Pure and Applied Physics, The Queen's University of Belfast, Belfast BT7 1NN, Northern Ireland*

[2]*Department of Applied Mathematics and Theoretical Physics, The Queen's University of Belfast, Belfast BT7 1NN, Northern Ireland*

[3]*Laboratory for Astronomy and Solar Physics, Code 682, NASA's Goddard Space Flight Center, Greenbelt, MD 20771, U.S.A.*

[4]*Department of Physics, The Catholic University of America, Washington, DC 20064, U.S.A.*

(Received 19 August 2003; accepted 28 December 2003)

Abstract. Recent R-matrix calculations of electron impact excitation rates in N-like Si VIII are used to derive theoretical emission line intensity ratios involving $2s^2 2p^3 - 2s2p^4$ transitions in the 216 – 320 Å wavelength range. A comparison of these with an extensive dataset of solar active region, quiet Sun, sub-flare and off-limb observations, obtained during rocket flights of the Solar EUV Research Telescope and Spectrograph (SERTS), indicates that the ratio R_1 = I(216.94 Å)/I(319.84 Å) may provide a usable electron density diagnostic for coronal plasmas. The ratio involves two lines of comparable intensity, and varies by a factor of about 5 over the useful density range of 10^8 – 10^{11} cm^{-3}. However R_2 = I (276.85 Å)/I(319.84 Å) and R_3 = I(277.05 Å)/I(319.84 Å) show very poor agreement between theory and observation, due to the severe blending of the 276.85 and 277.05 Å lines with Si VII and Mg VII transitions, respectively, making the ratios unsuitable as density diagnostics. The 314.35 Å feature of Si VIII also appears to be blended, with the other species contributing around 20% to the total line flux.

1. Introduction

Emission lines arising from transitions in N-like ions have been frequently detected in the spectra of astrophysical sources, including the Sun (see, for example, Thomas and Neupert, 1994 and references therein). The usefulness of these lines as plasma diagnostics was first noted over 50 years ago by Aller, Ufford, and Van Vleck (1949), in terms of deriving the electron density in gaseous nebulae. Feldman *et al.* (1978) subsequently showed that emission lines from N-like ions may also be employed as density diagnostics for solar plasmas.

Several authors have generated theoretical line ratios for N-like Si VIII applicable to solar spectra, calculated using electron impact excitation rates produced primarily in the Distorted-Wave approximation (see Bhatia and Landi, 2003; Keenan, 1996, and references therein). In this paper we present Si VIII line ratios determined with R-matrix electron excitation rates. We subsequently compare

Solar Physics **0:** 1–13, 2004.

these line ratios with other recent theoretical results, and also with an extensive dataset of several quiet and active region spectra, plus a sub-flare and an off-limb area, obtained with the Solar EUV Research Telescope and Spectrograph (SERTS).

2. Theoretical Line Ratios

The model ion for Si VIII consisted of the 11 energetically lowest LS states, namely $2s^2 2p^3\ ^4$S, ^{2}D and ^{2}P, $2s2p^4\ ^4$P, ^{2}D, ^{2}S, and ^{2}P, $2p^5\ ^2$P and $2s^2 2p^2 3s\ ^4$P, ^{2}P and ^{2}D, making a total of 22 fine-structure levels. Energies for all of these were taken from Martin and Zalubas (1983). Test calculations including higher-lying levels were found to have a negligible effect on the theoretical line ratios considered in this paper.

Electron impact excitation rates for transitions among the Si VIII levels discussed above have been calculated by Bell, Matthews, and Ramsbottom (2001) and Ramsbottom *et al.* (2003) using the R-matrix code as adapted for the Opacity Project (Berrington *et al.*, 1987; Seaton, 1987). These data include the effects of resonance structure on the collision strengths (in contrast to Distorted-Wave results), and hence should be the most accurate currently available. They have therefore been adopted in the present analysis.

Einstein A-coefficients for Si VIII were obtained from Bhatia and Landi (2003) for allowed lines, and Merkelis *et al.* (1999) for intercombination and forbidden transitions. Feldman *et al.* (1978) have pointed out that the inclusion of proton rates has a small effect on line ratio calculations for N-like ions. However for completeness we have included proton rates in our model ion, from Bhatia and Landi, for transitions among the $2s^2 2p^3$ levels.

Using the atomic data discussed above in conjunction with the statistical equilibrium code of Dufton (1977), relative Si VIII level populations and hence emission line strengths were calculated as a function of electron temperature (T_e) and density (N_e). Details of the procedures involved, and approximations made, may be found in Dufton (1977) and Dufton *et al.* (1978).

In Figures 1–3 we plot the theoretical emission line ratios

$$R_1 = \mathrm{I}(2s^2 2p^3\ ^2\mathrm{D}_{5/2} - 2s2p^{4\,2}\mathrm{P}_{3/2}) / I(2s^2 2p^3\ ^4\mathrm{S}_{3/2} - 2s2p^4\ ^4\mathrm{P}_{5/2})$$
$$= \mathrm{I}(216.94\ \text{Å})/\mathrm{I}(319.84\ \text{Å}),$$

$$R_2 = \mathrm{I}(2s^2 2p^3\ ^2\mathrm{D}_{3/2} - 2s2p^4\ ^2\mathrm{D}_{3/2,5/2})/\mathrm{I}(2s^2 2p^3\ ^4\mathrm{S}_{3/2} - 2s2p^4\ ^4\mathrm{P}_{5/2})$$
$$= \mathrm{I}(276.85\ \text{Å})/\mathrm{I}(319.84\ \text{Å}),$$

and

$$R_3 = \mathrm{I}(2s^2 2p^3\ ^2\mathrm{D}_{5/2} - 2s2p^4\ ^2\mathrm{D}_{3/2,5/2})/\mathrm{I}(2s^2 2p^3\ ^4\mathrm{S}_{3/2} - 2s2p^4\ ^4\mathrm{P}_{5/2})$$
$$= \mathrm{I}(277.05\ \text{Å})/\mathrm{I}(319.84\ \text{Å})$$

as a function of logarithmic electron density at the electron temperature of maximum Si VIII fractional abundance in ionization equilibrium, $T_{max} = 10^{5.9}$ K (Mazzotta *et al.*, 1998). Given errors in the adopted atomic data of typically ± 10% (see above references), we would expect the theoretical ratios to be accurate to better than ± 15%.

We note that the ratios

$$R_4 = \mathrm{I}(2s^2 2p^3\ {}^4\mathrm{S}_{3/2} - 2s2p^4\ {}^4\mathrm{P}_{1/2})/\mathrm{I}(2s^2 2p^3\ {}^4\mathrm{S}_{3/2} - 2s2p^4\ {}^4\mathrm{P}_{5/2})$$
$$= \mathrm{I}(314.35\ \text{Å})/\mathrm{I}(319.84\ \text{Å}),$$

and

$$R_5 = \mathrm{I}(2s^2 2p^3\ {}^4\mathrm{S}_{3/2} - 2s2p^4\ {}^4\mathrm{P}_{3/2})/\mathrm{I}(2s^2 2p^3\ {}^4\mathrm{S}_{3/2} - 2s2p^4\ {}^4\mathrm{P}_{5/2})$$
$$= \mathrm{I}(316.22\ \text{Å})/\mathrm{I}(319.84\ \text{Å})$$

are in the coronal approximation (Elwert, 1952) at the electron temperatures and densities considered in the present paper, and hence are predicted to have the constant values

$$R_4 = 0.348,$$

and

$$R_5 = 0.685.$$

An inspection of Figures 1–3 reveals that the R_1, R_2, and R_3 ratios are sensitive to variations in the electron density. For example, R_1 and R_3 vary by factors of over 5 between $N_e = 10^8$ and 10^{11} cm^{-3}, while R_2 changes by an order of magnitude over the same density interval. However we note that the ratios are relatively insensitive to changes in the adopted electron temperature. Decreasing T_e from $10^{5.9}$ K to $10^{5.6}$ K (i.e. by about 50%) leads to only a 21%, 2%, and 3% variation in R_1, R_2, and R_3, respectively, at $N_e = 10^8$ cm^{-3}. At $N_e = 10^{11}$ cm^{-3}, the changes due to the temperature decrease are still only 25% (R_1) and 10% (R_2 and R_3). This sensitivity to changes in the electron density, but not temperature, indicates that the ratios should (in principle) be useful N_e–diagnostics for the Si VIII emitting region of a plasma.

Also shown in Figures 1–3 are the theoretical line ratios generated using the latest version (4.01) of the CHIANTI database (Dere *et al.*, 1997; Young *et al.*, 2003), which differ by up to 40% from those presented here. These discrepancies are due primarily to the fact that our calculations employ R-matrix electron excitation rates for all transitions in Si VIII. By contrast, the CHIANTI results only use R-matrix data for transitions within the $2s^2 2p^3$ levels (Bell *et al.*, 2001), rates for all other transitions being those generated in the Distorted-Wave approximation (Zhang and Sampson, 1999; Bhatia and Landi, 2003). As noted by Ramsbottom *et al.* (2003), there are significant differences between the R-matrix and Distorted-Wave collision cross sections for several allowed transitions in Si VIII, including

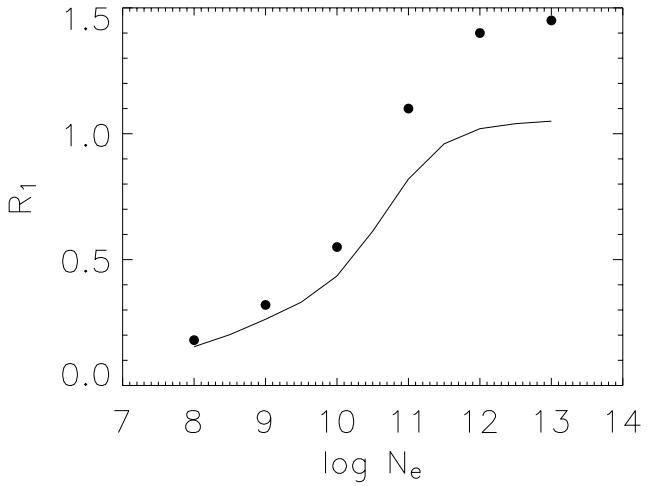

Figure 1. The theoretical Si VIII emission line ratio R_1 = I(216.94 Å)/I(319.84 Å), where I is in energy units, plotted as a function of logarithmic electron density (N_e in cm^{-3}) at the temperature of maximum Si VIII fractional abundance in ionization equilibrium, $T_{max} = 10^{5.9}$ K (Mazzotta *et al.*, 1998). The present calculations are shown as *solid lines*, while the *filled circles* are the results from the latest version (4.01) of the CHIANTI database.

those within the $2s^2 2p^3\ ^4S - 2s2p^4\ ^4P$ and $2s^2 2p^3\ ^2D - 2s2p^4\ ^2D$ multiplets. These discrepancies are due to the differing top-up procedures employed when evaluating the collision cross sections, particularly at high electron impact energies (see Ramsbottom *et al.* for more details).

3. Observational Data

The solar spectra analyzed in the present paper are those of several quiet and active regions, a small sub-flare, and an off-limb area, obtained with the SERTS instrument (Neupert *et al.* 1992). These spectra were recorded on Eastman Kodak 101–07 emulsion by SERTS during rocket flights on 5 May 1989 at 17:45 UT (SERTS-89), 7 May 1991 at 18:05 UT (SERTS-91), 17 August 1993 at 18:00 UT (SERTS-93) and 15 May 1995 at 18:00 UT (SERTS-95). For the rocket flight on 18 November 1997 at 19:35 UT (SERTS-97), an intensified CCD was employed as the detector. The spectral resolutions of the SERTS datasets are typically 50–80 mÅ (FWHM), apart from the SERTS-97 observations which have a resolution of 115 mÅ, while the spatial resolutions are about 7 arc sec (FWHM). Further details of the observations, and the wavelength and absolute flux calibration procedures employed in the data reduction, may be found in the following papers – SERTS-

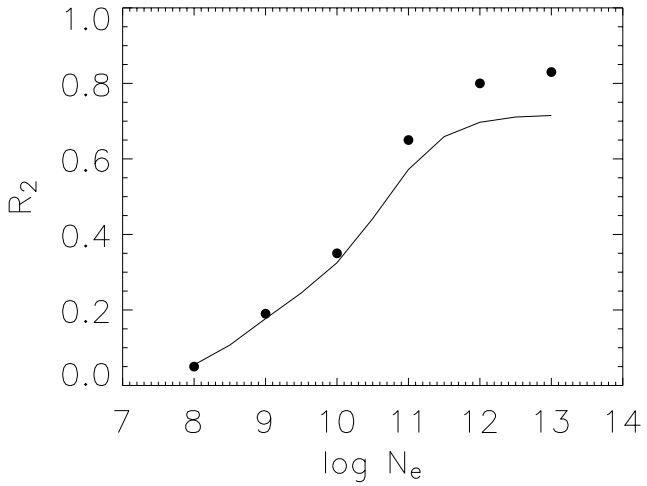

Figure 2. The theoretical Si VIII emission line ratio R_2 = I(276.85 Å)/I(319.84 Å), where I is in energy units, plotted as a function of logarithmic electron density (N_e in cm^{-3}) at the temperature of maximum Si VIII fractional abundance in ionization equilibrium, $T_{max} = 10^{5.9}$ K (Mazzotta *et al.*, 1998). The present calculations are shown as *solid lines*, while the *filled circles* are the results from the latest version (4.01) of the CHIANTI database.

89: Thomas and Neupert (1994); SERTS-91 and SERTS-93: Brosius *et al.* (1996); SERTS-95: Brosius, Davila, and Thomas (1998); SERTS-97: Brosius *et al.* (2000).

We have searched for Si VIII emission lines in the SERTS spectra, using the original line identifications by Thomas and Neupert (1994) for the SERTS-89 active region, as well as an additional transition (216.94 Å) found in this dataset by Dwivedi, Mohan, and Thomas (1998). In Table I we list the six Si VIII transitions identified in the SERTS spectra, along with the measured wavelengths. The line at 216.94 Å was observed in second spectral order, where the instrument's radiometric calibration is less certain; all others appeared in first-order. We note that the 276.85 and 277.05 Å features are each a blend of two components, namely $2s^2 2p^3\ ^2D_{3/2}-2s2p^4\ ^2D_{3/2} + 2s^2 2p^3\ ^2D_{3/2}-2s2p^4\ ^2D_{5/2}$ (276.85 Å), and $2s^2 2p^3\ ^2D_{5/2}-2s2p^4\ ^2D_{3/2} + 2s^2 2p^3\ ^2D_{5/2}-2s2p^4\ ^2D_{5/2}$ (277.05 Å). Thomas and Neupert only listed the major components of each feature ($2s^2 2p^3\ ^2D_{3/2}-2s2p^4\ ^2D_{3/2}$ and $2s^2 2p^3\ ^2D_{5/2}-2s2p^4\ ^2D_{5/2}$ for 276.85 and 277.05 Å, respectively). However the weaker blend can in fact contribute up to 10% of the total line flux.

In addition, Thomas and Neupert (1994) identified a line at 338.375 Å as being due to the $2s2p^4\ ^2P_{3/2}-2p^5\ ^2P_{1/2}$ transition of Si VIII. However Young, Landi, and Thomas (1998) subsequently dismissed this identification, as the Si VIII transition is not likely to have a significant intensity. This is confirmed by our line ratio

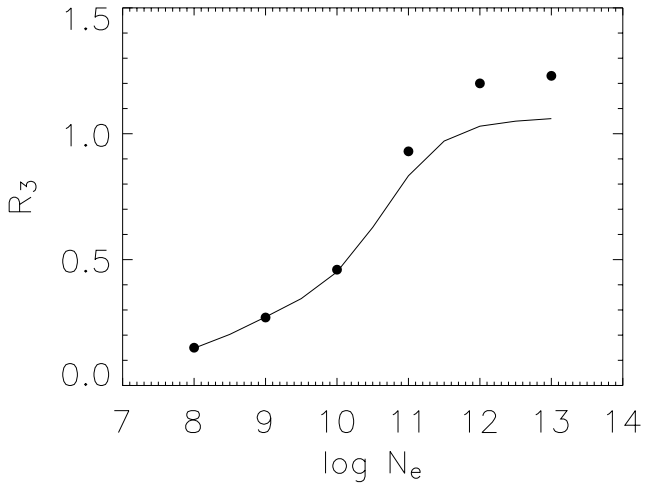

Figure 3. The theoretical Si VIII emission line ratio R_3 = I(277.05 Å)/I(319.84 Å), where I is in energy units, plotted as a function of logarithmic electron density (N_e in cm^{-3}) at the temperature of maximum Si VIII fractional abundance in ionization equilibrium, $T_{max} = 10^{5.9}$ K (Mazzotta *et al.*, 1998). The present calculations are shown as *solid lines*, while the *filled circles* are the results from the latest version (4.01) of the CHIANTI database.

TABLE I

Si VIII transitions identified in the SERTS spectra.

Transition	λ(Å)
$2s^2 2p^3\ ^2D_{5/2}$–$2s2p^4\ ^2P_{3/2}$	216.94
$2s^2 2p^3\ ^2D_{3/2}$–$2s2p^4\ ^2D_{3/2,5/2}$	276.85
$2s^2 2p^3\ ^2D_{5/2}$–$2s2p^4\ ^2D_{3/2,5/2}$	277.05
$2s^2 2p^3\ ^4S_{3/2}$–$2s2p^4\ ^4P_{1/2}$	314.35
$2s^2 2p^3\ ^4S_{3/2}$–$2s2p^4\ ^4P_{3/2}$	316.22
$2s^2 2p^3\ ^4S_{3/2}$–$2s2p^4\ ^4P_{5/2}$	319.84

calculations (Section 2), which indicate that the intensity of the Si VIII 338.375 Å line should be about a factor of 300 smaller than that measured in the SERTS-89 active region spectrum by Thomas and Neupert. The 338.375 Å line is therefore clearly not due to Si VIII. A search of the Atomic Line List of Peter van Hoof (star.pst.qub.ac.uk/∼pvh) reveals several possible identifications, such as the $3d^6\ ^5D_4$–$3d^5 4p\ ^5F_5$ or $3d^6\ ^5D_2$–$3d^5 4p\ ^5D_2$ transitions of Ni V.

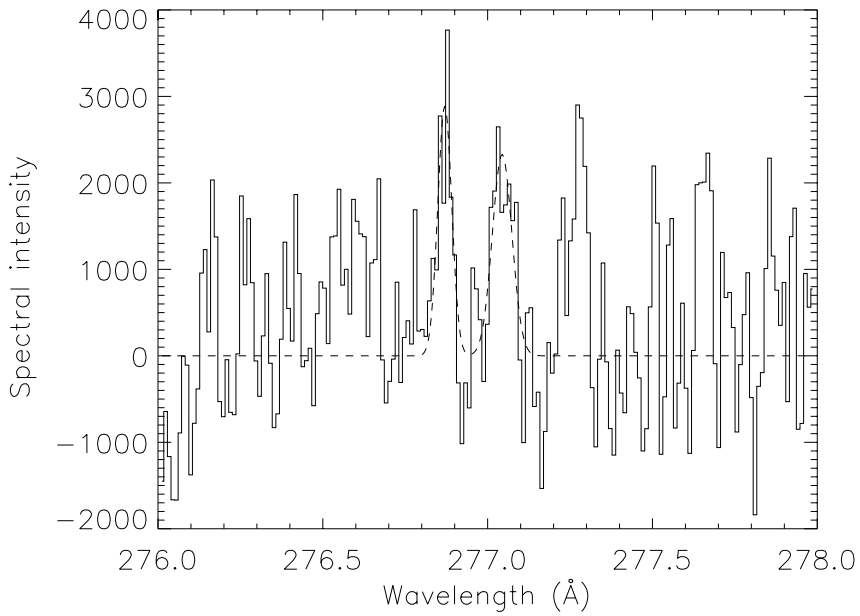

Figure 4. Plot of the SERTS–89 subflare spectrum in the 276.0–278.0 Å wavelength range, where the spectral intensity is in units of erg cm^{-2} s^{-1} sr^{-1} $Å^{-1}$. The profile fits to the Si VIII 276.85 Å and 277.05 Å features are shown by a dashed line. Also clearly visible in the figure is the Si X 277.27 Å emission line.

The quality of the observational data are illustrated in Figures 4–6, where we plot several portions of the SERTS spectra for a variety of solar features measured on different flights of the rocket payload. We note that an unidentified line at 316.13 Å lies in the wing of the Si VIII 316.22 Å feature, but the latter can be resolved and measured (see Figure 5). A possible identification for the 316.13 Å transition, from the Atomic Line List, is the $3d^6\ ^5D_3 - 3d^5 4p\ ^5D_3$ line of Ni V.

4. Results and Discussion

Intensities of the Si VIII lines in the SERTS spectra (where measurable) were determined by using the spectrum synthesis package DIPSO (Howarth, Murray, and Mills, 1994) to fit Gaussian profiles to the observations. The intensities of the 319.84 Å line are listed in Table II; the observed intensities of the other lines may be inferred from these using the line ratios given in Table III.

It should be pointed out that the SERTS-91 quiet-Sun intensity listed in Table II exceeds the active region value, which is ordinarily not the case. This is because,

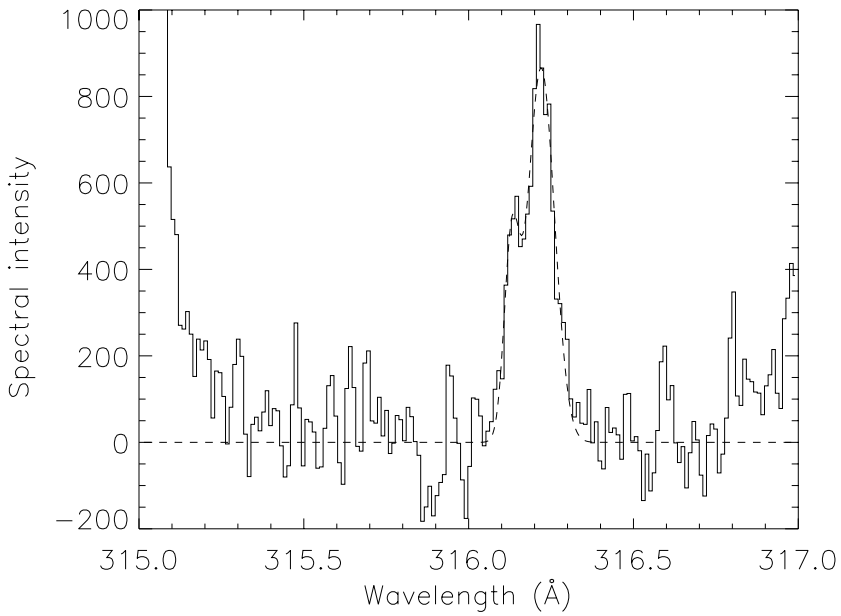

Figure 5. Plot of the SERTS–89 active region spectrum in the 315.0–317.0 Å wavelength range, where the spectral intensity is in units of erg cm^{-2} s^{-1} sr^{-1} $Å^{-1}$. The double Gaussian profile fit to the Si VIII 316.22 Å feature and an unidentified transition at 316.13 Å is shown by a dashed line. Also clearly visible in the figure is the Mg VIII 315.02 Å emission line.

TABLE II

Intensities of the Si VIII 319.84 Å emission line in the SERTS spectra.

Dataset	Solar feature	I(319.84 Å)[a]
SERTS-89	Active region	142.2 ± 17.5
SERTS-89	Subflare	204.3 ± 22.9
SERTS-91	Active region	33.2 ± 3.0
SERTS-91	Quiet Sun	101.5 ± 12.4
SERTS-91	Off-limb	92.0 ± 8.0
SERTS-93	Active region	146.5 ± 16.6
SERTS-93	Quiet Sun	35.8 ± 4.5
SERTS-95	Active region	90.0 ± 20.0
SERTS-97	Active region	92.2 ± 14.4

[a]Line intensities in units of erg cm^{-2} s^{-1} sr^{-1}.

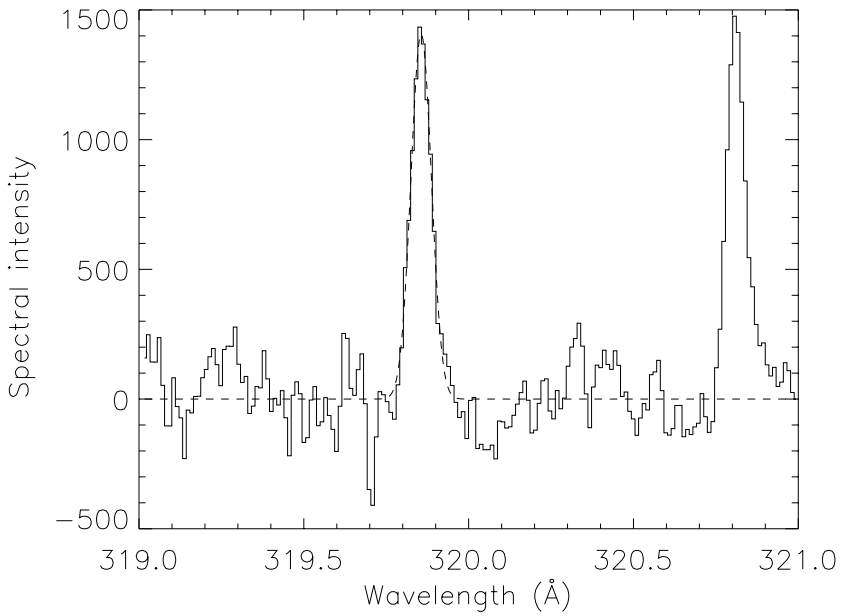

Figure 6. Plot of the SERTS–91 off-limb spectrum in the 319.0–321.0 Å wavelength range, where the spectral intensity is in units of erg cm^{-2} s^{-1} sr^{-1} $Å^{-1}$. The profile fit to the Si VIII 319.84 Å feature is shown by a dashed line. Also clearly visible in the figure is the Fe XIII 320.80 Å emission line.

on that flight, the emission labelled 'active region' was obtained from areas near, but not actually within, the most intense parts of the targeted source. Also, the quiet Sun intensity was measured over an area near the limb, where limb-brightening is significant for the Si VIII lines. Thus, the active region intensities are lower and the quiet Sun measurements are higher than typically reported values.

Observational uncertainties in the line intensities have been determined using methods discussed in detail by Thomas and Neupert (1994). The intensities and uncertainties quoted here are somewhat different from those originally reported in the papers referenced in Section 3, because the spectral data have been completely re-analysed by a standard fitting procedure to assure consistency of the results. Also, a uniform factor of 1.24 has been applied here to all SERTS-89 intensities, reflecting a more recent re-evaluation of its absolute calibration scale. Even so, in all but one of the directly comparable cases, the resulting intensity ratios differ only slightly from those obtained using previously published data.

The single exception to the above is the 316.22 Å line intensity in the SERTS-91 active region spectrum, for which Brosius *et al.* (1996) quote $I = 43.3 \pm 9.2$ erg cm^{-2} s^{-1} sr^{-1} for a broad feature at 316.195 Å. However, as noted in

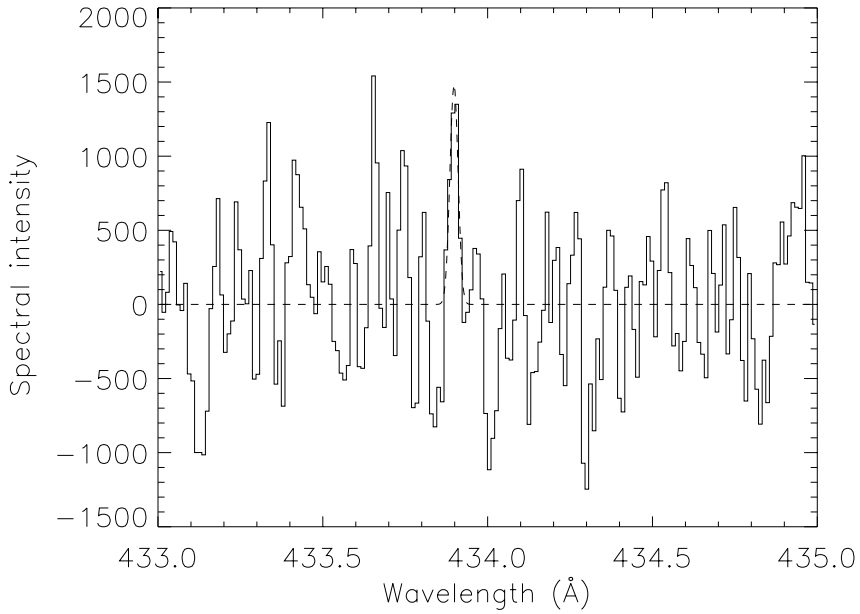

Figure 7. Plot of the SERTS–91 quiet Sun spectrum in the 433.0–435.0 Å wavelength range, where the spectral intensity is in units of erg cm^{-2} s^{-1} sr^{-1} $Å^{-1}$ (appropriate for first-order lines only). The profile fit to the Si VIII 216.94 Å feature (observed by SERTS in second-order at a wavelength of 2×216.94 = 433.88 Å) is shown by a dashed line.

Section 3, this feature actually consists of an unidentified transition at 316.13 Å with I = 17.0 ± 5.4 erg cm^{-2} s^{-1} sr^{-1}, and the Si VIII line at 316.22 Å with I = 24.4 ± 4.3 erg cm^{-2} s^{-1} sr^{-1}.

In Table III we list the Si VIII emission line intensity ratios measured from the SERTS spectra, along with the associated 1σ errors. Also given in the table are the theoretical results for R_1, R_2, and R_3 from Figures 1–3, at electron densities derived for the SERTS solar features from emission line ratios in Si IX, Si X, Fe XI or Fe XII (Keenan *et al.*, 1996, 2000, 2003; Brosius *et al.*, 1996, 1998, 2000). All of these species have temperatures of maximum fractional abundance in ionization equilibrium of $T_{max} = 10^{6.1}$ K (Mazzotta *et al.*, 1998), close to that for Si VIII. Hence densities derived from these ions should reflect that of the Si VIII emitting plasma in the solar feature. For R_4 and R_5, which are not predicted to be N_e–sensitive, the theoretical results in Table III are the values listed in Section 2.

An inspection of Table III reveals generally very poor agreement between theory and observation for R_2 and R_3. Young *et al.* (1998) note that the 276.85 Å line of Si VIII in the SERTS-89 active region spectrum is blended with the $2s^2 2p^4$ $^3P_0$–$2s2p^5$ $^3P_1$ transition of Si VII at 276.84 Å, while Si VIII 277.05 Å similarly

TABLE III

Si VIII emission line ratios in the SERTS spectra.

dataset	Solar feature	Ratio	Observed	Theoretical[a]
SERTS-89	Active region	R_1	0.27 ± 0.15	0.33
SERTS-89	Active region	R_2	0.58 ± 0.17	0.28
SERTS-89	Active region	R_3	0.75 ± 0.22	0.39
SERTS-89	Active region	R_4	0.48 ± 0.11	0.35
SERTS-89	Active region	R_5	0.78 ± 0.14	0.69
SERTS-89	Subflare	R_2	0.57 ± 0.25	0.29
SERTS-89	Subflare	R_3	1.0 ± 0.24	0.41
SERTS-89	Subflare	R_4	0.40 ± 0.16	0.35
SERTS-89	Subflare	R_5	0.80 ± 0.20	0.69
SERTS-91	Active region	R_2	2.3 ± 0.70	0.26
SERTS-91	Active region	R_5	0.73 ± 0.14	0.69
SERTS-91	Quiet Sun	R_2	1.1 ± 0.60	0.23
SERTS-91	Quiet Sun	R_4	0.31 ± 0.08	0.35
SERTS-91	Quiet Sun	R_5	0.63 ± 0.12	0.69
SERTS-91	Off-limb	R_4	0.51 ± 0.12	0.35
SERTS-91	Off-limb	R_5	0.77 ± 0.15	0.69
SERTS-93	Active region	R_2	0.46 ± 0.24	0.23
SERTS-93	Active region	R_4	0.38 ± 0.07	0.35
SERTS-93	Active region	R_5	0.76 ± 0.13	0.69
SERTS-93	Quiet Sun	R_4	0.51 ± 0.09	0.35
SERTS-93	Quiet Sun	R_5	0.72 ± 0.13	0.69
SERTS-95	Active region	R_2	0.78 ± 0.35	0.23
SERTS-95	Active region	R_4	0.33 ± 0.10	0.35
SERTS-95	Active region	R_5	0.67 ± 0.38	0.69
SERTS-97	Active region	R_4	0.40 ± 0.09	0.35
SERTS-97	Active region	R_5	0.78 ± 0.17	0.69

[a] R_1, R_2, and R_3 ratios calculated at the electron temperature of maximum Si VIII fractional abundance in ionization equilibrium, $T_{max} = 10^{5.9}$ K (Mazzotta *et al.*, 1998), and at electron densities appropriate to the relevant SERTS solar feature, namely: SERTS-89 active region – $N_e = 10^{9.7}$ cm^{-3}; SERTS-89 subflare – $N_e = 10^{9.8}$ cm^{-3}; SERTS-91 active region – $N_e = 10^{9.6}$ cm^{-3}; SERTS-91 quiet Sun – $N_e = 10^{9.4}$ cm^{-3}; SERTS-93 active region – $N_e = 10^{9.4}$ cm^{-3}; SERTS-95 active region – $N_e = 10^{9.4}$ cm^{-3}.

has a significant contribution from the $2s^2 2p^2\ ^3P_1 - 2s2p^3\ ^3S_1$ feature of Mg VII at 277.00 Å. Our results indicate that this blending is prevalent throughout the SERTS datasets, and indeed in some instances can be very severe. For example, in the SERTS-91 active region spectrum, R_2 is nearly a factor of 10 larger than predicted, indicating that in this instance the Si VII line is the dominant contributor to the

Si VII/VIII 276.85 Å blend. Similarly, R_3 in the SERTS-89 subflare spectrum is over a factor of 2 larger than the theoretical value, implying that Mg VII is responsible for more than 50% of the measured 277.05 Å line flux. Clearly, R_2 and R_3 are not suitable for use as N_e–diagnostics, at least in solar plasmas.

However for the sole measurement of R_1, from the SERTS-89 active region spectrum, there is good agreement between theory and observation. Since R_1 involves the 216.94 Å line measured by SERTS-89 in second spectral order, this result gives added confidence to the relative radiometric calibrations of the instrument around that wavelength. It also indicates that R_1 may provide a useful electron density indicator for coronal plasmas, involving lines of comparable magnitude. We note that we have also identified the 216.94 Å line of Si VIII in the SERTS-91 quiet Sun spectrum, shown in Figure 7. Unfortunately, we are unable to accurately measure the line intensity (and hence produce a reliable value for R_1), due to the lack of an adequate second-order intensity calibration for the SERTS-91 flight. That flight featured the first ever use of a multilayer-coated grating tuned to enhance first-order sensitivity, which then led to a reduced second-order response.

In the case of R_4 and R_5, there also appears to be consistency between the experimental and theoretical results. However as these ratios are predicted to be constant, we can extend this comparison by averaging the measured data. For observed R_4 and R_5 ratios with uncertainities of less than 25%, we find mean values of $\overline{R_4} = 0.46 \pm 0.06$ and $\overline{R_5} = 0.74 \pm 0.06$, while the theoretical results are $R_4 = 0.35$ and $R_5 = 0.69$. The R_5 ratio shows good agreement between theory and observation, but the R_4 comparison suggests that the Si VIII 314.35 Å line may be blended, with the other species contributing perhaps 20% to the total line flux. A possible identification for this blend, from the Atomic Line List, is the $3d^6\ ^3F_1 - 3d^5 4p\ ^3F_0$ line of Ni V.

Acknowledgements

ACK acknowledges financial support from the Leverhulme Trust via grant F/00203/A. The SERTS rocket programme is supported by RTOP grants from the Solar Physics Office of NASA's Space Physics Division. JWB acknowledges additional NASA support under grant NAG5-13321. FPK is grateful to AWE Aldermaston for the award of a William Penney Fellowship. The authors thank Peter van Hoof for the use of his Atomic Line List, and Anand Bhatia for a copy of his Si VIII atomic data in advance of publication.

References

Aller, L. H., Ufford, C. W., and Van Vleck, J. H.: 1949, *Astrophys. J.* **109**, 42.

Bell, K. L., Matthews, A., and Ramsbottom, C. A.: 2001, *Monthly Notices Royal Astron. Soc.* **322**, 779.

Berrington, K. A., Burke, P. G., Butler, K., Seaton, M. J., Storey, P. J., Taylor, K. T., and Yan, Y.: 1987, *J. Phys.* **B20**, 6379.
Bhatia, A. K. and Landi, E.: 2003, *Atomic Data Nucl. Data Tables*, in press.
Brosius, J. W., Davila, J. M., and Thomas, R. J.: 1998, *Astrophys. J. Suppl.* **119**, 255.
Brosius, J. W., Davila, J. M., Thomas, R. J., and Monsignori-Fossi, B. C.: 1996, *Astrophys. J. Suppl.* **106**, 143.
Brosius, J. W., Thomas, R. J., Davila, J. M., and Landi, E.: 2000, *Astrophys. J.* **543**, 1016.
Dere, K. P., Landi, E., Mason, H. E., Monsignori-Fossi, B. C., and Young, P. R.: 1997, *Astron. Astrophys. Suppl.* **125**, 149.
Dufton, P. L.: 1977, *Comp. Phys. Comm.* **13**, 25.
Dufton, P. L., Berrington, K. A., Burke, P. G., and Kingston, A. E.: 1978, *Astron. Astrophys.* **62**, 111.
Dwivedi, B., Mohan, A., and Thomas, R. J.: 1998, *Solar Phys.* **180**, 157.
Elwert, G.: 1952, *Z. Naturforsch.* **7A**, 432.
Feldman, U., Doschek, G. A., Mariska, J. T., Bhatia, A. K., and Mason, H. E.: 1978, *Astrophys. J.* **226**, 674.
Howarth, I. D., Murray, J., and Mills, D.: 1994, *Starlink User Note No. 50.15*.
Keenan, F. P.: 1996, *Space Sci. Rev.* **75**, 537.
Keenan, F. P., Katsiyannis, A. C., Aggarwal, K. M., Mathioudakis, M., Brosius, J. W., Davila, J. M., and Thomas, R. J.: 2003, *Solar Phys.* **212**, 65.
Keenan, F. P., O'Shea, E., Thomas, R. J., Brosius, J. W., Katsiyannis, A. C., Ryans, R. S. I., Reid, R. H. G., Pradhan, A. K., and Zhang, H. L.: 2000, *Monthly Notices Royal Astron. Soc.* **315**, 450.
Keenan, F. P., Thomas, R. J., Neupert, W. M., Foster, V. J., Brown, P. J. F., and Tayal, S. S.: 1996, *Monthly Notices Royal Astron. Soc.* **278**, 773.
Martin, W. C. and Zalubas, R.: 1983, *J. Phys. Chem. Ref. Data* **12**, 323.
Mazzotta, P., Mazzitelli, G., Colafrancesco, S., and Vittorio, N.: 1998, *Astron. Astrophys. Suppl.* **133**, 403.
Merkelis, G., Martinson, I., Kisielius, R., and Vilkas, M. J.: 1999, *Phys. Scripta* **59**, 122.
Neupert, W. M., Epstein, G. L., Thomas, R. J., and Thompson, W. T.: 1992, *Solar Phys.* **137**, 87.
Ramsbottom, C. A., Bell, K. L., Keenan, F. P., and Matthews, A.: 2003, *Atomic Data Nucl. Data Tables* **85**, 69.
Seaton, M. J.: 1987, *J. Phys.* **B20**, 6363.
Thomas, R. J. and Neupert, W. M.: 1994, *Astrophys. J. Suppl.* **91**, 461.
Young, P. R., Del Zanna, G., Landi, E., Dere, K. P., Mason, H. E., and Landini, M.: 2003, *Astrophys. J. Suppl.* **144**, 135.
Young, P. R., Landi, E., and Thomas, R. J.: 1998, *Astron. Astrophys.* **329**, 291.
Zhang, H. L. and Sampson, D. H.: 1999, *Atomic Data Nucl. Data Tables* **72**, 153.